Free Vibration Behavior of Spinning Shear-Deformable Plates Composed of Composite Materials

R. Bhumbla,* J. B. Kosmatka,† and J. N. Reddy‡
Virginia Polytechnic Institute and State University, Blacksburg, Virginia 24061

A first-order shear-deformation plate theory is used to predict the free vibration frequencies and mode shapes in spinning laminated composite plates. The theory accounts for geometric nonlinearity in the form of the von Kármán strains and the effects of rotatory inertia. The plate is permitted to have an arbitrary orientation offset from the axis of rotation. A finite element model is developed to obtain numerical solutions to this class of problems. The model is validated by comparing the results for isotropic plates with those available in literature. The natural frequencies and mode shapes of isotropic and laminated composite plates as functions of angular velocity, pitch angle, and sweep angle are presented. Though the expected increase in frequency with angular velocity is observed for most modes, it is seen that there is a decrease in the free vibration frequency with angular velocity for torsional modes of swept and pitched plates.

Introduction

IN recent years, there has been a renewed interest in the design of aircraft turbopropellers that have much higher fuel efficiency than present aircraft engines.[1] This is because of the availability of composite materials that have high strength-to-weight ratios. The composite blades can be manufactured in a mold, therefore, it is possible to produce complex geometries that result in quiet, efficient propellers. Also the properties of the laminated composites can be varied by changing their layup. Thus, the composite blades can be designed to have a predetermined static and dynamic behavior.

Earlier studies of vibrations in spinning blades considered beam-type models for their analyses as these studies were carried out for helicopter blades. The dynamic behavior of turbopropellers has been studied by Kosmatka and Friedmann,[2,3] Subrahmanyam and Kaza,[4] Mehmed et al.,[5] and Maser et al.[6]

Since low-aspect ratio blades tend to behave like plates rather than beams, it is expected that a plate model will provide better results for propellers with high width-to-length ratios. Dokainish and Rawtani,[7] Ramamurti and Kielb,[8] Wang et al.,[9] and Shaw et al.[10] have studied vibrations in rotating plates. Only Refs. 8 and 9 have studied behavior of laminated composite plates, but they have neglected the Coriolis effects.

Gupta,[11] Meirovitch,[12] and Bauchau[13] have developed algorithms to solve the eigenvalue problem associated with the free vibration of spinning structures. Bauchau found that the stiffness matrix for the problem was composed of three components: the linear stiffness matrix, the nonlinear stiffness matrix due to spin-induced loads, and the centrifugal stiffness matrix. The nonlinear and the centrifugal stiffnesses vanish when the plate is not spinning. Besides this, there is a gyroscopic matrix due to the Coriolis acceleration. The stiffness and mass matrices for this problem are symmetric, whereas the gyroscopic matrix is skew-symmetric.

The objective of the present paper is to study the free vibration behavior of spinning plates while considering transverse shear deformation and rotatory inertia. A displacement finite element model based on the first-order shear deformation plate theory is developed to obtain numerical solutions of the governing equations for a spinning plate. Some features of the model are the following:

1) The plate is permitted to have fixed translational and rotational offsets from the axis of rotation (Fig. 1).

2) The laminated composite plate is permitted to have plies with arbitrary orientation, and each ply is permitted to have different orthotropic material properties.

3) Aerodynamic loads on the plate have not been considered; therefore, the plate modeled is physically equivalent to one rotating in a vacuum. (In future studies, aerodynamic loads can be brought into consideration by making minor alterations to the present development.)

4) A first-order, nonlinear theory of plates with transverse shear deformation has been used for the analysis. This theory incorporates geometrical nonlinearity in the form of von Kármán strains (see Refs. 14–16).

In the first-order shear deformation plate theory,[17] the displacements are assumed to vary linearly through the thickness. The transverse shear strains and, hence, the transverse shear stresses are constant through the thickness. Actually, the transverse shear stresses are observed to vary parabolically through the thickness and are zero at the plate surfaces. Reissner[18] and Mindlin[19] have attempted to correct this shortcoming by multiplying the transverse shear forces by a constant, the shear correction factor, to make the strain energy of the

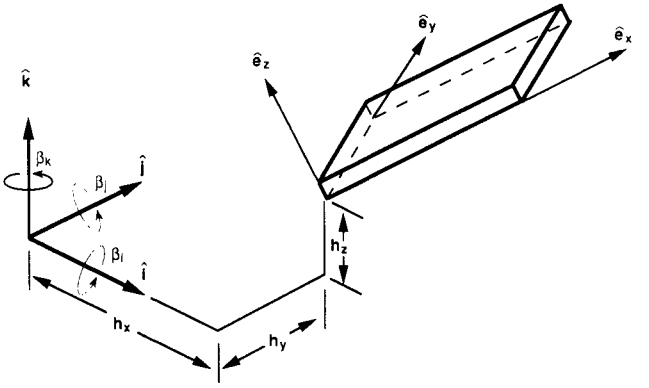

Fig. 1 Rotational and translational offsets of plate coordinate axes from the inertial axes.

Received Sept. 11, 1989; revision received January 23, 1990.

*Graduate Research Assistant; currently at University of California, San Diego.

†Assistant Professor; currently at University of California, San Diego. Member AIAA.

‡Clifton C. Garvin Professor.

plate closer to that obtained using a parabolic stress distribution. The value of shear correction factor given by Reissner, 5/6, is used in this study.

Theoretical Development

According to the first-order shear-deformation theory, the in-plane displacements are assumed to vary linearly through the thickness, i.e., displacements are functions of first-order powers of the thickness coordinate z. Thus, the displacement field for a first-order shear deformation theory can be expressed as[14-17]

$$u(x,y,z,t) = u_0(x,y,t) + z\psi_x(x,y,t) \tag{1a}$$

$$v(x,y,z,t) = v_0(x,y,t) + z\psi_y(x,y,t) \tag{1b}$$

$$w(x,y,z,t) = w_0(x,y,t) \tag{1c}$$

where u_0, v_0, and w_0 are the displacements at the midplane and ψ_x and ψ_y are the rotations about y and $-x$ axes, respectively. Note that w is assumed to be constant through the thickness, implying that the transverse normal strain is zero.

Using the von Kármán theory of plates (which assumes the derivatives of in-plane displacements are much smaller than the corresponding out-of-plane terms and, thus, neglects products and squares of derivatives of in-plane displacements) and the displacement field [Eqs. (1)], the following strain-displacement relations can be derived (see Refs. 14–16):

$$\epsilon_x = \frac{\partial u_0}{\partial x} + z\frac{\partial \psi_x}{\partial x} + \tfrac{1}{2}\left(\frac{\partial w_0}{\partial x}\right)^2 \tag{2a}$$

$$\epsilon_y = \frac{\partial v_0}{\partial y} + z\frac{\partial \psi_y}{\partial y} + \tfrac{1}{2}\left(\frac{\partial w_0}{\partial y}\right)^2 \tag{2b}$$

$$\epsilon_z = 0 \tag{2c}$$

$$\gamma_{xy} = \frac{\partial u_0}{\partial y} + \frac{\partial v_0}{\partial x} + z\left(\frac{\partial \psi_x}{\partial y} + \frac{\partial \psi_y}{\partial x}\right) + \frac{\partial w_0}{\partial x}\frac{\partial w_0}{\partial y} \tag{2d}$$

$$\gamma_{yz} = \psi_y + \frac{\partial w_0}{\partial y} \tag{2e}$$

$$\gamma_{xz} = \psi_x + \frac{\partial w_0}{\partial x} \tag{2f}$$

For a plate composed of orthotropic plies with an arbitrary orientation, using the first-order shear-deformation plate theory assumption of negligible transverse normal stress, the constitutive relations for each ply are obtained in global coordinates to be[17,20]

$$\begin{Bmatrix} \sigma_x \\ \sigma_y \\ \tau_{xy} \\ \tau_{yz} \\ \tau_{xz} \end{Bmatrix}^{(m)} = \begin{bmatrix} \bar{Q}_{11} & \bar{Q}_{12} & \bar{Q}_{16} & 0 & 0 \\ \bar{Q}_{12} & \bar{Q}_{22} & \bar{Q}_{26} & 0 & 0 \\ \bar{Q}_{16} & \bar{Q}_{26} & \bar{Q}_{66} & 0 & 0 \\ 0 & 0 & 0 & \bar{Q}_{44} & \bar{Q}_{45} \\ 0 & 0 & 0 & \bar{Q}_{45} & \bar{Q}_{55} \end{bmatrix}^{(m)} \begin{Bmatrix} \epsilon_x \\ \epsilon_y \\ \gamma_{xy} \\ \gamma_{yz} \\ \gamma_{xz} \end{Bmatrix} \tag{3}$$

where (m) denotes the mth ply in the laminated plate and $\bar{Q}_{ij}^{(m)}$ are the plane stress-reduced stiffness coefficients for the laminae.

The stress resultants are given by

$$\begin{Bmatrix} N_x \\ N_y \\ N_{xy} \end{Bmatrix} = \sum_{m=1}^{n} \int_{z_m}^{z_{m+1}} \begin{Bmatrix} \sigma_x \\ \sigma_y \\ \tau_{xy} \end{Bmatrix}^{(m)} dz \tag{4}$$

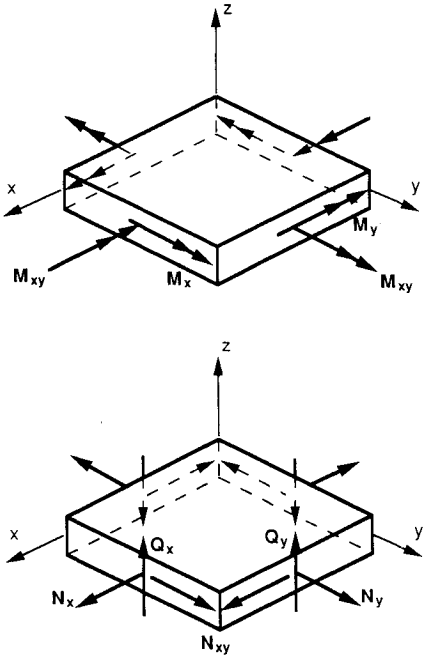

Fig. 2 Force and moment resultants.

where z_m is the distance of the bottom of the mth ply from the midplane of the plate and n is the number of plies in the laminate.

Similarly, the moment and the shear force resultants are given by

$$\begin{Bmatrix} M_x \\ M_y \\ M_{xy} \end{Bmatrix} = \sum_{m=1}^{n} \int_{z_m}^{z_{m+1}} \begin{Bmatrix} \sigma_x \\ \sigma_y \\ \tau_{xy} \end{Bmatrix}^{(m)} z\, dz$$

$$\begin{Bmatrix} Q_y \\ Q_x \end{Bmatrix} = \sum_{m=1}^{n} \int_{z_m}^{z_{m+1}} \begin{Bmatrix} \tau_{yz} \\ \tau_{xz} \end{Bmatrix}^{(m)} dz \tag{5}$$

The positive directions of the force and moment resultants are shown in Fig. 2.

Substituting the strain-displacement relations [Eqs. (2)] and the constitutive relations [Eq. (3)] into the previous equations for the stress resultants, the following expressions are obtained:

$$\begin{Bmatrix} N_x \\ N_y \\ N_{xy} \\ M_x \\ M_y \\ M_{xy} \\ Q_y \\ Q_x \end{Bmatrix} = \begin{bmatrix} A_{11} & A_{12} & A_{16} & B_{11} & B_{12} & B_{16} & 0 & 0 \\ A_{12} & A_{22} & A_{26} & B_{12} & B_{22} & B_{26} & 0 & 0 \\ A_{16} & A_{26} & A_{66} & B_{16} & B_{26} & B_{66} & 0 & 0 \\ B_{11} & B_{12} & B_{16} & D_{11} & D_{12} & D_{16} & 0 & 0 \\ B_{12} & B_{22} & B_{26} & D_{12} & D_{22} & D_{26} & 0 & 0 \\ B_{16} & B_{26} & B_{66} & D_{16} & D_{26} & D_{66} & 0 & 0 \\ 0 & 0 & 0 & 0 & 0 & 0 & \bar{A}_{44} & \bar{A}_{45} \\ 0 & 0 & 0 & 0 & 0 & 0 & \bar{A}_{45} & \bar{A}_{55} \end{bmatrix} \begin{Bmatrix} \{\epsilon^0\} + \{\epsilon^{NL}\} \\ \{\kappa\} \\ \{\gamma^0\} \end{Bmatrix} \tag{6}$$

where $\{\epsilon^0\}^T = \{\epsilon_x^0, \epsilon_y^0, \gamma_{xy}^0\}^T$ are the linear midplane strains given by

$$\epsilon_x^0 = \frac{\partial u_0}{\partial x}, \qquad \epsilon_y^0 = \frac{\partial v_0}{\partial y}, \qquad \gamma_{xy}^0 = \frac{\partial u_0}{\partial y} + \frac{\partial v_0}{\partial x} \tag{7a}$$

$\{\epsilon^{NL}\}^T = \{\epsilon_x^{NL}, \epsilon_y^{NL}, \gamma_{xy}^{NL}\}^T$ are the nonlinear midplane strains,

$$\epsilon_x^{NL} = \tfrac{1}{2}\left(\frac{\partial w_0}{\partial x}\right)^2, \quad \epsilon_y^{NL} = \tfrac{1}{2}\left(\frac{\partial w_0}{\partial y}\right)^2, \quad \gamma_{xy}^{NL} = \frac{\partial w_0}{\partial x}\frac{\partial w_0}{\partial y} \tag{7b}$$

$\{\kappa\}^T = \{\kappa_x, \kappa_y, \kappa_{xy}\}^T$ are the midplane curvatures,

$$\kappa_x = \frac{\partial \psi_x}{\partial x}, \qquad \kappa_y = \frac{\partial \psi_y}{\partial y}, \qquad \kappa_{xy} = \frac{\partial \psi_x}{\partial y} + \frac{\partial \psi_y}{\partial x} \tag{7c}$$

and $\{\gamma^0\}^T = \{\gamma^0_{yz}, \gamma^0_{xz}\}^T$ are the shearing strains,

$$\gamma^0_{yz} = \psi_y + \frac{\partial w_0}{\partial y}, \qquad \gamma^0_{xz} = \psi_x + \frac{\partial w_0}{\partial x} \tag{7d}$$

Also, the laminate stiffness coefficients are defined as

$$(A_{ij}, B_{ij}, D_{ij}) = \sum_{m=1}^{n} \int_{z_m}^{z_{m+1}} \bar{Q}^{(m)}_{ij}(1, z, z^2)\, dz$$

$$\bar{A}_{ij} = k^2 A_{ij}, \qquad i,j = 4,5$$

here, k^2 is the shear correction factor (taken to be 5/6).

The equations of motion for the spinning plate are derived via Hamilton's principle where the variation in the time integral of the Lagrangian function is set to zero:

$$\delta \int_{t_1}^{t_2} (U - T - W_e)\, dt = 0 \tag{8}$$

where U is the plate strain energy, T is the plate kinetic energy, and W_e the plate external work.

The strain energy for an elastic system having plane normal stress is given by

$$U = \tfrac{1}{2} \int_A \int_{-h/2}^{h/2} (\sigma_x \epsilon_x + \sigma_y \epsilon_y + \tau_{xy}\gamma_{xy} + \tau_{yz}\gamma_{yz} + \tau_{xz}\gamma_{xz})\, dz\, dA \tag{9}$$

The variation in the strain energy δU is determined by substituting Eqs. (4-7) into Eq. (9) and taking the variation with respect to the unknowns u_0, v_0, w_0, ψ_x, and ψ_y:

$$\begin{aligned}\delta U = -\int_A \Bigg\{ &\left(\frac{\partial N_x}{\partial x} + \frac{\partial N_{xy}}{\partial y}\right)\delta u_0 + \left(\frac{\partial N_y}{\partial y} + \frac{\partial N_{xy}}{\partial x}\right)\delta v_0 \\ &+ \left[\frac{\partial}{\partial x}\left(N_x \frac{\partial w_0}{\partial x} + N_{xy}\frac{\partial w_0}{\partial y}\right) + \frac{\partial Q_x}{\partial x} \right. \\ &\left. + \frac{\partial}{\partial y}\left(N_y \frac{\partial w_0}{\partial y} + N_{xy}\frac{\partial w_0}{\partial x}\right) + \frac{\partial Q_y}{\partial y}\right]\delta w_0 \\ &+ \left(\frac{\partial M_x}{\partial x} + \frac{\partial M_{xy}}{\partial y} - Q_x\right)\delta \psi_x \\ &+ \left(\frac{\partial M_y}{\partial y} + \frac{\partial M_{xy}}{\partial x} - Q_y\right)\delta \psi_y \Bigg\}\, dA\end{aligned} \tag{10}$$

The total kinetic energy of a plate can be expressed as

$$T = \tfrac{1}{2} \int_A \int_{-h_2}^{h_2} \rho\, V \cdot V\, dz\, dA \tag{11}$$

where ρ is the mass density of the plate and V the velocity vector of an arbitrary point on the plate with respect to the inertial reference frame $(\hat{I},\hat{J},\hat{K})$. It is assumed that the plate rotates about the inertial coordinate system $(\hat{I},\hat{J},\hat{K})$, with an angular velocity Ω about the $\hat{K}$ axis:

$$V = \frac{dr}{dt} + \Omega \hat{K} \times r \tag{12}$$

where r is the position vector from the origin of the inertial reference frame to a point on the deformed plate

$$r = (h_i, h_j, h_k)\begin{Bmatrix} \hat{I} \\ \hat{J} \\ \hat{K} \end{Bmatrix} + (x + u, y + v, z + w)\begin{Bmatrix} \hat{e}_x \\ \hat{e}_y \\ \hat{e}_z \end{Bmatrix} \tag{13}$$

where (h_i, h_j, h_k) are fixed translational offsets of the plate coordinate axes $(\hat{e}_x, \hat{e}_y, \hat{e}_z)$ from the inertial axes $(\hat{I}, \hat{J}, \hat{K})$, as shown in Fig. 1, (x,y,z) are the coordinates of the point in the plate coordinate system (the plate element being in $\hat{e}_x - \hat{e}_y$ plane, $z = 0$ for each element), and (u,v,w) are the elastic deflections of a point on the plate.

Substituting the displacement definitions [Eqs. (1)] into the position vector [Eq. (13)] and transforming to the local coordinate axes $(\hat{e}_x, \hat{e}_y, \hat{e}_z)$,

$$r = (h_x + x + u_0 + z\psi_x,\ h_y + y + v_0 + z\psi_y,\ h_z + w_0)\begin{Bmatrix} \hat{e}_x \\ \hat{e}_y \\ \hat{e}_z \end{Bmatrix} \tag{14}$$

where $(h_x, h_y, h_z) = (h_i, h_j, h_k)[T_{LG}]^T$, and $[T_{LG}]$ is the transformation matrix between the two sets of axes obtained by rotations through the Euler angles β_i, β_j, β_k about the axes $\hat{I}$, $\hat{J}$, and $\hat{K}$, respectively. The order of rotations is β_k, β_j, and β_i.

Similarly, $\Omega\hat{K}$ can be written in the plate coordinate system as

$$\Omega\hat{K} = \Omega_x \hat{e}_x + \Omega_y \hat{e}_y + \Omega_z \hat{e}_z \tag{15}$$

where

$$(\Omega_x, \Omega_y, \Omega_z) = (0,0,\Omega)[T_{LG}]^T$$

The velocity vector V of Eq. (12) is calculated using Eqs. (14) and (15):

$$\begin{aligned} V = &[(\dot{u}_0 + z\dot{\psi}_x) + \Omega_y(h_z + w_0) - \Omega_z(h_y + y + v_0 + z\psi_y)]\hat{e}_x \\ &+ [(\dot{v}_0 + z\dot{\psi}_y) + \Omega_z(h_x + x + u_0 + z\psi_x) - \Omega_x(h_z + w_0)]\hat{e}_y \\ &+ [\dot{w}_0 + \Omega_x(h_y + y + v_0 + z\psi_y) - \Omega_y(h_x + x + u_0 \\ &+ z\psi_x)]\hat{e}_z \end{aligned} \tag{16}$$

Using Eqs. (11) and (16), the kinetic energy variation can be obtained as

$$\delta T = \int_A (\bar{Z}u_0\, \delta u_0 + \bar{Z}v_0\, \delta v_0 + \bar{Z}w_0\, \delta w_0 + \bar{Z}\psi_x\, \delta\psi_x + \bar{Z}\psi_y\, \delta\psi_y)\, dA \tag{17}$$

where $\bar{Z}u_0$, $\bar{Z}v_0$, $\bar{Z}w_0$, $\bar{Z}\psi_x$, $\bar{Z}\psi_y$ are obtained in Ref. [21] and defined in Appendix A.

The governing equations are obtained by substituting Eqs. (10) and (17) into Eq. (8), where the work due to external forces W_e has been neglected:

$$\delta u_0: \quad \frac{\partial N_x}{\partial x} + \frac{\partial N_{xy}}{\partial y} + \bar{Z}u_0 = 0 \tag{18a}$$

$$\delta v_0: \quad \frac{\partial N_y}{\partial y} + \frac{\partial N_{xy}}{\partial x} + \bar{Z}v_0 = 0 \tag{18b}$$

$$\begin{aligned}\delta w_0: \quad &\frac{\partial}{\partial x}\left(N_x \frac{\partial w_0}{\partial x} + N_{xy}\frac{\partial w_0}{\partial y}\right) \\ &+ \frac{\partial}{\partial y}\left(N_y \frac{\partial w_0}{\partial y} + N_{xy}\frac{\partial w_0}{\partial x}\right) \\ &+ \frac{\partial Q_y}{\partial y} + \frac{\partial Q_x}{\partial x} + \bar{Z}w_0 = 0\end{aligned} \tag{18c}$$

$$\delta\psi_x: \quad \frac{\partial M_x}{\partial x} + \frac{\partial M_{xy}}{\partial y} - Q_x - \bar{Z}\psi_x = 0 \tag{18d}$$

$$\delta\psi_y: \quad \frac{\partial M_y}{\partial y} + \frac{\partial M_{xy}}{\partial x} - Q_y - \bar{Z}\psi_y = 0 \tag{18e}$$

Finite Element Model

In the present analysis, the displacement finite element model based on the total Lagrangian functional (8) is formulated (see Refs. 16 and 17). The displacements u_0, v_0, w_0, ψ_x, and ψ_y are interpolated using expressions of the form:

$$u_0 = \sum_{j=1}^{ne} q_j^1 \phi_j, \qquad v_0 = \sum_{j=1}^{ne} q_j^2 \phi_j,$$

$$w_0 = \sum_{j=1}^{ne} q_j^3 \phi_j, \qquad \psi_x = \sum_{j=1}^{ne} q_j^4 \phi_j,$$

$$\psi_y = \sum_{j=1}^{ne} q_j^5 \phi_j \tag{19}$$

where ϕ_j are the Lagrange interpolation functions associated with the rectangular plate elements, q_j^i are the nodal values of u_0, v_0, w_0, ψ_x, and ψ_y, respectively, at the jth node of the element, and n_e is the number of nodes in each element.

Substituting these interpolations into Eq. (18), the following nonlinear equations of motion are obtained

$$[M]\{\ddot{q}\} + [C]\{\dot{q}\} + ([K^L] + [K^{CF}] + [K^{NL}(q)])\{q\} = \{F^{CF}\} \tag{20}$$

where $[M]$ is the mass matrix, $[C]$ the gyroscopic matrix, $[K^L]$ the geometrically linear stiffness matrix, $[K^{NL}]$ the geometrically nonlinear stiffness matrix, and $[K^{CF}]$ and $\{F^{CF}\}$ the stiffness matrix and the force vector, respectively, due to the centrifugal terms. The $[M]$, $[K^L]$, $[K^{CF}]$ are symmetric matrices and $[C]$ is a skew-symmetric matrix. The details of the formulation of $[K^{CF}]$, $[C]$, and $\{F^{CF}\}$ are presented in Appendix B. The shear stiffness coefficients are evaluated using reduced integration to avoid numerical locking (see Ref. 17). The nonlinear stiffness matrix $[K^{NL}]$ increases the plate stiffness as a result of centrifugal loading, whereas the centrifugal stiffness matrix $[K^{CF}]$ reduces the plate stiffness in the rotational plane of the spinning plate (centrifugal softening). Thus, the increases in the natural frequencies of the spinning plate are more pronounced for vibrations out of the rotational plane (flapping motion) than in the rotational plane (lead-lag motion).

The equations of motion are solved in two parts: the determination of the static shape and the vibrations about this nonlinear static position.

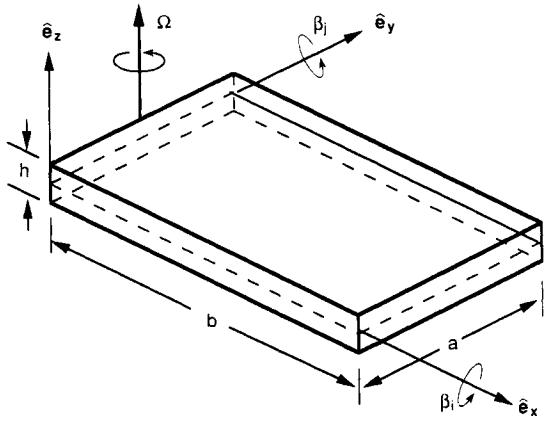

Fig. 3 Plate geometry, spin axis, and plate rotations.

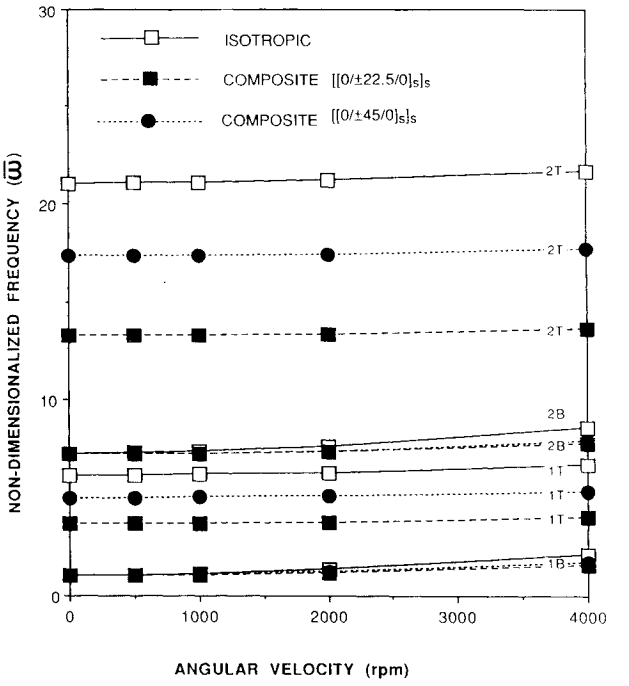

Fig. 4 Comparison of natural frequencies using current approach and Ref. 10.

Static Analysis

For the static analysis, the time-dependent terms are neglected in Eq. (20), and the following form is obtained

$$[K^L + K^{CF} + K^{NL}(q_s)]\{q_s\} = \{F^{CF}\} \tag{21}$$

where $\{q_s\}$ is the static component of the deflections. The Newton-Raphson method is used to solve the above algebraic form of the nonlinear differential equations.

Dynamic Analysis

For the dynamic analysis, both the static and the time-dependent components of Eq. (20) are considered, where the displacement vector $\{q\}$ can be expressed as the sum of a static and a dynamic term. Thus,

$$\{q\} = \{q_s\} + \{\delta(t)\}$$

where $\{q_s\}$ is the nonlinear static equilibrium solution as a result of the centrifugal load, and $\{\delta\}$ is a small linear time-dependent perturbation about the static displaced position.

The equations of motion can be written in terms of the static and dynamic terms as

$$[M]\{\ddot{\delta}\} + [C]\{\dot{\delta}\} + [K^L + K^{CF} + K^{NL}(q_s + \delta)]\{q_s + \delta\} = \{F^{CF}\} \tag{22}$$

On substituting the first-order Taylor series expansion of $[K^{NL}(q_s + \delta)]$ about $\{q_s\}$, and Eq. (21) into Eq. (20), and neglecting products of the perturbation quantities (i.e., $\delta \cdot \delta \simeq 0$) the following equations of motion are obtained

$$[M]\{\ddot{\delta}\} + [C]\{\dot{\delta}\} + [K^T]\{\delta\} = \{0\} \tag{23}$$

where $[K^T]$ is the tangent stiffness matrix evaluated at the nonlinear static equilibrium position at the plate and defined as

$$[K^T] = [K^L] + [K^{CF}] + \frac{\partial}{\partial q}([K^{NL}(q)]\{q\})\,|_{q=q_s} \tag{24}$$

Equation (23) is the standard form of the equations of motion of undamped free vibrations of spinning structures, as the [C] matrix previously obtained represents the gyroscopic (Coriolis) effects rather than the damping terms. The previous equations of motion can be rewritten in first-order form:

$$[A]\{\dot{s}\} - [B]\{s\} = \{0\}$$

where

$$[A] = \begin{bmatrix} [M] & [0] \\ [0] & [K^T] \end{bmatrix}, \qquad [B] = \begin{bmatrix} [0] & [M] \\ -[M] & -[C] \end{bmatrix}$$

and

$$\{s\} = \begin{Bmatrix} \{\dot{\delta}\} \\ \{\delta\} \end{Bmatrix} \tag{25}$$

Here, [A] is symmetric and [B] is antisymmetric. Taking the solution to be of the form $s = ce^{\lambda t}$ (where c is an arbitrary constant), Eq. (25) can be rewritten as

$$[B]^{-1}[A]\{s\} = \lambda[I]\{s\} \tag{26}$$

Thus, the eigenvalues of $[B]^{-1}[A]$ are also the eigenvalues of the problem under consideration. Equation (26) represents a first-order eigenvalue problem. It has complex eigenvalues, with the real part denoting exponential growth or decay (depending on sign) and the imaginary part being the harmonic component. However, because the present study does not consider damping or aerodynamic loads, the eigenvalues are purely imaginary; the imaginary part is the free vibration frequency of the plate.

Numerical Results and Discussion

The numerical results were obtained on an IBM 3090 computer using a 4 × 4 finite element mesh of linear Lagrangian rectangular finite elements described in Ref. 22. Natural frequencies and mode shapes as functions of angular velocity, pitch angle (β_i), and sweep angle (β_j) have been tabulated for spinning cantilever plates composed of isotropic and laminated composite materials. The plate analyzed has the geometry shown in Fig. 3, where a, b, and h represent the length, width, and overall thickness of the plate, respectively. The plate has clamped boundary conditions along one edge ($x = 0$), which is imposed by restraining the in-plane u_0, v_0 and transverse w_0 displacements and the rotation normal to the clamped edge ψ_x. The spin axis is taken to be at the center of the clamped edge and the angular velocity of the plate Ω is constant.

Verification Studies

The natural frequencies of the spinning isotropic plate were calculated and compared to the linear analytical predictions of Ref. 10. The nonlinearities of the current approach were suppressed for this particular study in order to provide a meaningful comparison. The plate is square with a side-to-thickness ratio of 10 (thick plate) and material properties given by $E = 70.0$ GPa, $\nu = .30$, and $\rho = 3.0 \times 10^3$ Kg/m^3. In addition, the spin axis is defined as perpendicular to the plane of the plate so that both the pitch β_i and sweep β_j angles are equal to zero.

The first five natural frequencies of the spinning plate as a function of angular (spin) velocity are presented in Fig. 4. For the verification study, the angular velocity Ω has been nondimensionalized to the first natural frequency of the nonrotating plate and the plate natural frequency ω is nondimensionalized using the relation $\bar{\omega}' = \omega a^2\sqrt{\rho h/D}$, where $D = Eh^3/12(1-\nu^2)$. The labels 1B and 2B represent the first and second out-of-plane bending modes (flapping motion), 1T and 2T are the first and second torsion modes, and 1L is the first in-plane bending mode (lead-lag motion). The current results are in excellent agreement with Ref. 10 for the fundamental out-of-plane bending (1B) and torsion (1T) modes. They are measurably lower than the results of Ref. 10 for the next three modes (2B, 1L, 2T). This discrepancy occurs because the current model is developed using a shear deformation theory, whereas the model of Ref. 10 is based on classical plate theory (Kirchhoff assumptions) that neglects the effect of shear deformation. Thus, the current mode predicts more accurately the stiffness of this thick plate, whereas the model of Ref. 10 overpredicts the stiffness and natural frequencies.

Additional numerical results that validate the nonlinear static and linear dynamic behavior of the current plate model

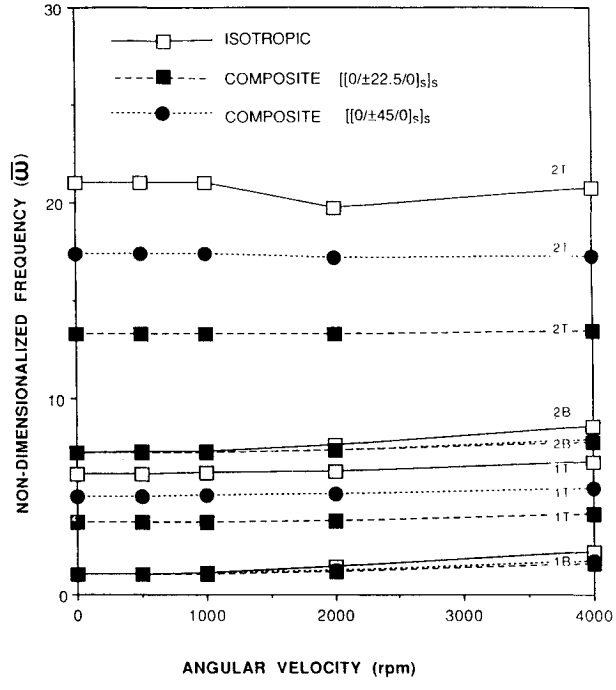

Fig. 5 Variation of frequency with angular velocity of isotropic and laminated composite plates (pitch angle = 0 deg, sweep angle = 0 deg).

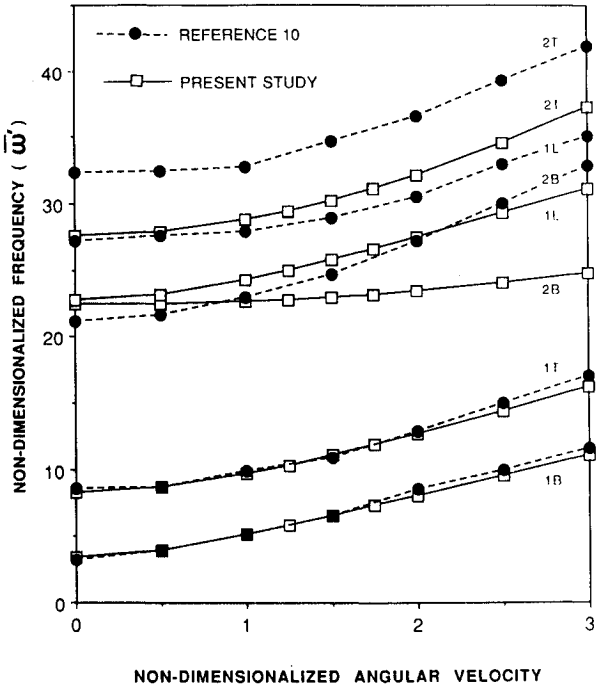

Fig. 6 Variation of frequency with angular velocity of isotropic and laminated composite plates (pitch angle = 22.5 deg, sweep angle = 0 deg).

are presented in Ref. 21. Numerical results are presented in Ref. 21 to show complete agreement between this study and Ref. 10 for thin isotropic plates (side-to-thickness ratio > 20), where the effects associated with shear deformation are negligible.

Current Studies

The free vibration behavior of a spinning isotropic plate as a function of angular velocity for various pitch angle β_i and sweep angle β_j settings has been studied. The thin rectangular plate has a length (a) of 228.6 mm, a width (b) of 76.2 mm, and a thickness (h) of 2.4 mm. The material properties of the plate are $E = 68.95$ GPa, $\nu = 0.33$, and $\rho = 2.713 \times 10^3$ Kg/m^3.

The first four vibration frequencies as a function of angular velocity for an unpitched ($\beta_i = 0.0$ deg) and unswept ($\beta_j = 0.0$ deg) spinning plates are presented in Fig. 5, where the vibration frequencies are nondimensionalized to the fundamental free vibration frequency of the nonrotating plate ($\bar{\omega} = \omega/\omega_{NR}$). The fundamental free vibration frequency for the nonrotating plate are the following: isotropic plate = 242.47, $[[0/\pm 22.5/0]_s]_s$ laminated composite plate = 396.07, and $[[0/\pm 45/0]_s]_s$ laminated composite plate = 341.25. Clearly, the centrifugal force distribution for this setting affects the out-of-plane bending natural frequencies more than the torsion natural frequencies. In Fig. 6, the natural frequencies are presented for a spinning plate with a finite pitch setting ($\beta_i = 22.5$ deg). The variation in the natural frequencies as a function of angular velocity is nearly identical to the unpitched plate for the first bending and torsion modes of the plate (Fig. 5). Thus, the introduction of pitch setting has little effect on straight flat plates for the lower modes. However, a decrease in frequency is observed for the second torsion mode (2T) for the plate with pitch. This decrease is observed only at low angular velocities after which the centrifugal effects become apparent and the expected increase in frequency with angular velocity is seen.

Introducing a finite sweep angle ($\beta_j = 22.5$ deg) has a pronounced effect on the free vibration characteristics of unpitched (Fig. 7) and pitched (Fig. 8) spinning plates. The first three natural frequencies experience a monotonic increase that is much less dramatic than the increase found in unswept plates (see Figs. 5 and 6). In addition, the natural frequency

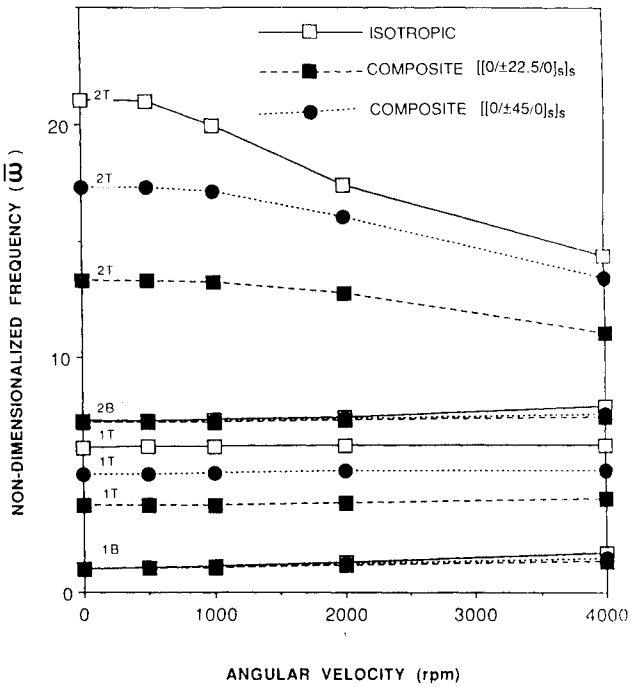

Fig. 7 Variation of frequency with angular velocity of isotropic and laminated composite plates (pitch angle = 0 deg, sweep angle = 0 deg).

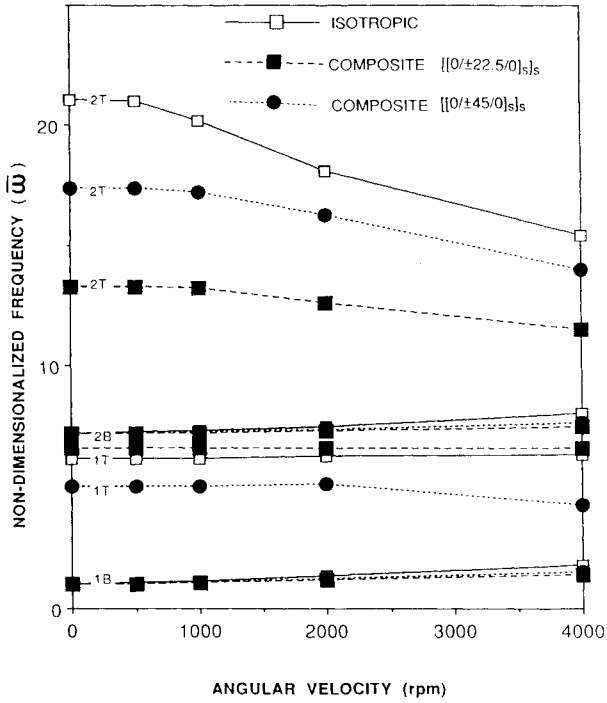

Fig. 8 Variation of frequency with angular velocity of isotropic and laminated composite plates (pitch angle = 22.5 deg, sweep angle = 22.5 deg).

associated with the second torsion mode undergoes a significant reduction with increasing angular velocity. These characteristics occur because the centrifugal force distribution acting on the plate has components parallel and normal to its surface. The parallel (in-plane) components directly increase the plate stiffness, whereas the normal (out-of-plane) components produce plate bending that alters the deformed plate shape (nonlinear static equilibrium position) and the plate stiffness.

The first four mode shapes of the nonrotating plate along with similar mode shapes for a spinning plate ($\Omega = 4000$ rpm) at three different pitch and sweep settings are presented in Fig. 9. The solid line on the plate platform represents a nodal line (line of zero motion) and the dashed line defines the outline of the in-plane mode shape. Modes 1 and 3 are the first (1B) and second (2B) out-of-plane bending modes of the plate, where the nodal lines are defined at the blade root for the 1B mode and at the blade root and near the three-quarter span for the 2B mode. Modes 2 and 4 are the first (1T) and second (2T) torsion modes, where the nodal line runs along the plate centerline for the 1T mode and has a t-type pattern for the 2T mode. The introduction of plate sweep β_j produces coupling between the flexural and in-plane motions of the plate that is more apparent in the torsion modes than in the bending modes.

The free vibration characteristics of two different spinning laminated composite plates were also investigated. The graphite/epoxy plates have different ply layups, $[[0/\pm 22.5/0]_s]_s$ vs $[[0/\pm 45/0]_s]_s$, but their built-up external geometries (16 plies) are identical to the isotropic plate ($a = 228.6$ mm, $b = 76.2$ mm, $h = 2.4$ mm). This was done to provide a direct comparison with the isotropic plate results. The orthotropic material properties of a graphite/epoxy ply are defined as $E_1 = 132.3$ GPa, $E_2 = 10.75$ GPa, $\nu_{12} = .239$, $G_{12} = G_{13} = 5.65$ GPa, $G_{23} = 5.84$ GPa and $\rho = 1.6 \times 10^3$ Kg/m^3.

The free vibration frequencies as a function of angular velocity for different combinations of pitch ($\beta_i = 0.0$ and 22.5 deg) and sweep ($\beta_j = 0.0$ and 22.5 deg) angle settings are presented in Figs. 5–8, where the frequencies are nondimensionalized to the fundamental free vibration frequency of the nonrotating plate. For the unswept ($\beta_j = 0.0$) plate with either no-pitch ($\beta_i = 0.0$; Fig. 5) or finite pitch ($\beta_i = 22.5$ deg; Fig. 6)

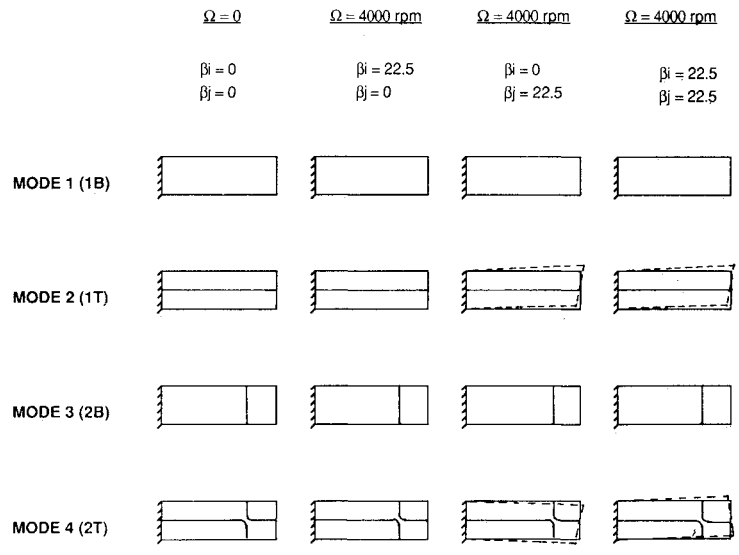

Fig. 9 Mode shapes of isotropic plates.

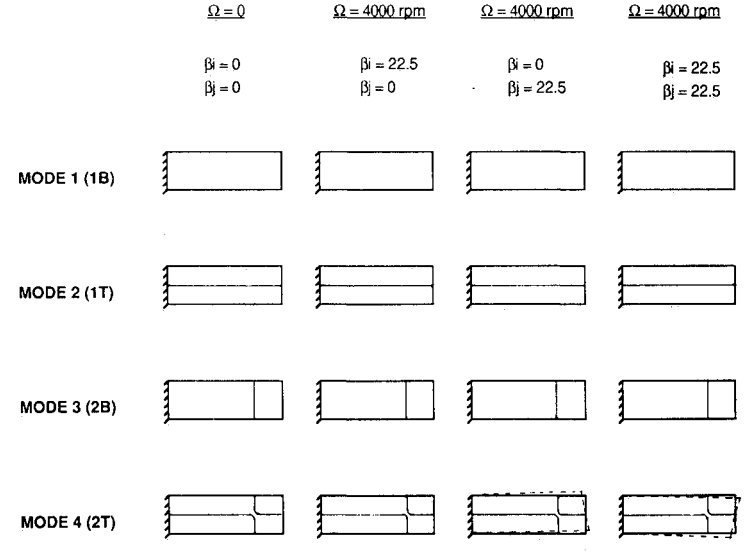

Fig. 10 Mode shapes of laminated composite plates.

setting, the behavior of the laminated composite plates is similar to the isotropic plate. Changing the angle plies from ± 45 to ± 22.5 significantly increases the bending stiffness, thus, the bending (1B, 2B) natural frequencies are less effected by the centrifugal forces. In addition, the ratio of the torsion stiffness to bending stiffness is reduced, which lowers the nondimensionalized torsion (1T, 2T) natural frequencies.

When the spinning laminated composite plates are given either a finite sweep ($\beta_j = 22.5$ deg; Fig. 7) or a combined pitch and sweep ($\beta_i = 22.5$ deg, $\beta_j = 22.5$ deg; Fig. 8), their out-of-plane bending (1B, 2B) frequencies resemble the general trends of the isotropic plate. The vibration characteristics of the torsion natural frequencies can be quite different. For example, the first torsion (1T) frequency of both plates undergoes a slight increase for the unpitched and swept setting (like the isotropic plate), whereas this same frequency experiences a decrease for the ± 45 deg angle ply (unlike the ± 22.5 deg angle-ply plate or the isotropic plate) for the combined pitch and sweep setting. The frequency reduction associated with the second torsion (2T) mode generally agrees with the isotropic plate for both pitch settings of the swept plate. The percentage reduction is less for the laminated composite plates and the angle ply of $\pm$ 22.5 deg because of its large bending stiffness.

The mode shapes of the nonrotating and rotating ($\Omega = 4000$ rpm) laminated composite plates are presented in Fig. 10. The torsion modes of the spinning swept plate undergo complex flexural and in-plane motions similar to the isotropic plate. This coupled motion is not readily visible in the out-of-plane bending modes.

Conclusions

An analytical model has been developed for determining the free vibration characteristics of spinning laminated composite plates. The model is sufficiently general to allow for any combination of layered orthotropic plies, and the resulting laminated plate can be arbitrarily oriented in space relative to the spin axis. The model incorporates a first-order shear de-

formation plate theory with geometric nonlinearities in the form of the von Kármán strains.

From the results obtained, it is noted that there is an increase in the free vibration frequencies of a spinning plate with an increase in angular velocity. This increase is present for all modes of an unswept plate regardless of the pitch setting. For plates with sweep, there is a significant reduction in the free vibration frequency of the higher torsions modes with increasing angular velocity. The percentage reduction in the frequency is lower for laminated composite plates than for isotropic plates. For plates with combined pitch and sweep, the vibration frequency associated with the fundamental torsion mode may either increase or decrease depending on the ply orientation. The mode shapes associated with the spinning swept plate have coupling between the flexural and in-plane motions that is more apparent in the torsion modes than in the out-of-plane bending modes.

These results describe how a typical laminated composite plate may perform. Obviously, different ply configurations would change the frequency predictions and the mode shape definitions. This model can be used as a basis for analysts developing refined theories for the nonlinear dynamic or aeroelastic behavior of spinning laminated composite plates.

Appendix A

The coefficients associated with δu_0, δv_0, δw_0, $\delta\psi_x$, and $\delta\psi_y$ obtained in the expression for variation in the plate kinetic energy [Eq. (17)] are the following:

$$\bar{Z}u_0 = I_1[-\ddot{u}_0 - 2\Omega_y\dot{w}_0 + 2\Omega_z\dot{v}_0 + (\Omega_y^2+\Omega_z^2)(h_x+x+u_0) - \Omega_z\Omega_x(h_z+w_0) - \Omega_y\Omega_x(h_y+y+v_0)]$$
$$+ I_2[-\ddot{\psi}_x + 2\Omega_z\dot{\psi}_y + (\Omega_y^2+\Omega_z^2)\psi_x - \Omega_y\Omega_x\psi_y] \tag{A1}$$

$$\bar{Z}v_0 = I_1[-\ddot{v}_0 - 2\Omega_z\dot{u}_0 + 2\Omega_x\dot{w}_0 + (\Omega_z^2+\Omega_x^2)(h_y+y+v_0) - \Omega_z\Omega_y(h_z+w_0) - \Omega_x\Omega_y(h_x+x+u_0)]$$
$$+ I_2[-\ddot{\psi}_y - 2\Omega_z\dot{\psi}_x + (\Omega_z^2+\Omega_x^2)\psi_y - \Omega_x\Omega_y\psi_x] \tag{A2}$$

$$\bar{Z}w_0 = I_1[-\ddot{w}_0 - 2\Omega_x\dot{v}_0 + 2\Omega_y\dot{u}_0 + (\Omega_x^2+\Omega_y^2)(h_z+w_0) - \Omega_y\Omega_z(h_y+y+v_0) - \Omega_x\Omega_z(h_x+x+u_0)]$$
$$+ I_2(-2\Omega_x\dot{\psi}_y + 2\Omega_y\dot{\psi}_x - \Omega_y\Omega_z\psi_y - \Omega_x\Omega_z\psi_x) \tag{A3}$$

$$\bar{Z}\psi_x = I_2[-\ddot{u}_0 - 2\Omega_y\dot{w}_0 + 2\Omega_z\dot{v}_0 + (\Omega_y^2+\Omega_z^2)(h_x+x+u_0) - \Omega_z\Omega_x(h_z+w_0) - \Omega_y\Omega_x(h_y+y+v_0)]$$
$$+ I_3[-\ddot{\psi}_x + 2\Omega_z\dot{\psi}_y + (\Omega_y^2+\Omega_z^2)\psi_y - \Omega_y\Omega_x\psi_y] \tag{A4}$$

$$\bar{Z}\psi_y = I_2[-\ddot{v}_0 - 2\Omega_z\dot{u}_0 + 2\Omega_x\dot{w}_0 + (\Omega_z^2+\Omega_x^2)(h_y+y+v_0) - \Omega_z\Omega_y(h_z+w_0) - \Omega_x\Omega_y(h_x+x+u_0)]$$
$$+ I_3[-\ddot{\psi}_y - 2\Omega_z\dot{\psi}_x + (\Omega_z^2+\Omega_x^2)\psi_y - \Omega_x\Omega_y\psi_x] \tag{A5}$$

where

$$(I_1,I_2,I_3) = \sum_{m=1}^{n}\int_{z_m}^{z_{m+1}} \rho_m(1,z,z^2)\,dz \tag{A6}$$

ρ_m is the mass density of the mth ply in the laminate.

Appendix B

The stiffness matrix $[K^{CF}]$, the coriolis matrix $[C]$, and the force vector $\{F^{CF}\}$ associated with the centrifugal effects are given as

$$[K^{CF}] = \int_A [N]^T[\bar{K}^{CF}][N]\,dA \tag{B1}$$

$$[C] = \int_A [N]^T[\bar{C}][N]\,dA \tag{B2}$$

$$\{F^{CF}\} = \int_A [N]^T\{\bar{F}^{CF}\}\,dA \tag{B3}$$

where

$$[\bar{K}^{CF}] = \begin{bmatrix} -I_1(\Omega_y^2+\Omega_z^2) & I_1(\Omega_y\Omega_x) & I_1(\Omega_z\Omega_x) & -I_2(\Omega_y^2+\Omega_z^2) & I_2(\Omega_y\Omega_x) \\ I_1(\Omega_y\Omega_x) & -I_1(\Omega_x^2+\Omega_z^2) & I_1(\Omega_z\Omega_y) & I_2(\Omega_x\Omega_y) & -I_1(\Omega_z^2+\Omega_x^2) \\ I_1(\Omega_x\Omega_z) & I_1(\Omega_y\Omega_z) & -I_1(\Omega_x^2+\Omega_y^2) & I_2(\Omega_x\Omega_z) & I_2(\Omega_y\Omega_z) \\ -I_2(\Omega_y^2+\Omega_z^2) & I_2(\Omega_y\Omega_x) & I_2(\Omega_x\Omega_z) & -I_3(\Omega_y^2+\Omega_z^2) & I_3(\Omega_y\Omega_x) \\ I_2(\Omega_y\Omega_x) & -I_2(\Omega_z^2+\Omega_x^2) & I_2(\Omega_z\Omega_y) & I_3(\Omega_x\Omega_y) & -I_3(\Omega_z^2+\Omega_x^2) \end{bmatrix} \tag{B4}$$

$$[\bar{C}] = \begin{bmatrix} 0 & -2I_1\Omega_z & 2I_1\Omega_y & 0 & -2I_2\Omega_z \\ 2I_1\Omega_z & 0 & -2I_1\Omega_x & 2I_2\Omega_z & 0 \\ -2I_1\Omega_y & 2I_1\Omega_x & 0 & -2I_2\Omega_y & 2I_2\Omega_x \\ 0 & -2I_2\Omega_z & 2I_2\Omega_y & 0 & -2I_3\Omega_z \\ 2I_2\Omega_z & 0 & -2I_2\Omega_x & 2I_3\Omega_z & 0 \end{bmatrix} \tag{B5}$$

$$[\bar{F}^{CF}] = \begin{bmatrix} I_1[(\Omega_y^2 + \Omega_z^2)(h_x + x) - \Omega_z\Omega_x h_z - \Omega_y\Omega_x(h_y + y)] \\ I_1[(\Omega_z^2 + \Omega_x^2)(h_y + y) - \Omega_z\Omega_y h_z - \Omega_x\Omega_y(h_x + x)] \\ I_1[(\Omega_x^2 + \Omega_y^2)h_z - \Omega_y\Omega_z(h_y + y) - \Omega_x\Omega_z(h_x + x)] \\ I_2[(\Omega_y^2 + \Omega_z^2)(h_x + x) - \Omega_z\Omega_x h_z - \Omega_y\Omega_x(h_y + y)] \\ I_2[(\Omega_z^2 + \Omega_x^2)(h_y + y) - \Omega_z\Omega_y h_z - \Omega_x\Omega_y(h_x + x)] \end{bmatrix} \tag{B6}$$

$[N]$ are the standard Lagrangian shape functions, as described in Ref. 22.

References

[1]Whitlow, J. B., Jr., and Sievers, G. K., "Fuel Savings Potential of NASA Advanced Turboprop Program," NASA-TM 83736, Sept. 1984.

[2]Kosmatka, J. B., and Friedmann, P. P., "Vibration Analysis of Composite Turbo-Propellors Using a Nonlinear Beam-Type Finite Element Approach," *AIAA Journal,* Vol. 27, No. 11, 1989, pp. 1606–1614.

[3]Kosmatka, J. B., and Friedman, P. P., "Structural Dynamic Modelling of Advanced Composite Turbo-propellers by the Finite Method," *Proceedings of the 28th AIAA/ASME/AHS/ASCE Structures, Structural Dynamics and Materials Conference,* AIAA, Washington, DC, Vol. 2, 1987, pp. 111–124.

[4]Subrahmanyam, K. B., and Kaza, K. R. V., "Vibration and Buckling of Rotating, Pretwisted, Preconed Beams Including Coriolis Effects," *Journal of Vibration, Stress and Reliability in Design,* Vol. 108, April 1986, pp. 140–149.

[5]Mehmed, O., Kaza, K. R. V., Lubomski, J. F., and Kielb, R. E., "Bending-Torsion Flutter of a Highly Swept Advanced Turboprop," NASA TM 82975, Oct. 1982.

[6]Maser, J. G., Fertis, D. G., Aiello, R. A., and Chamis, C. C., "Parametric Studies of Advanced Turboprops," *Proceedings of the AIAA/ASME/AHS/ASCE 29th Structures, Structural Dynamics, and Materials Conference,* AIAA, Washington, DC, Vol. 1, 1988, pp. 431–440.

[7]Dokainish, M. A., and Rawtani, S., "Vibration Analysis of Rotating Cantilever Plates," *International Journal for Numerical Methods in Engineering,* Vol. 3, No. 2, 1971, pp. 233–248.

[8]Ramamurti, V., and Kielb, R., "Natural Frequencies of Twisted Rotating Plates," *Journal of Sound and Vibration,* Vol. 97, No. 3, 1984, pp. 429–449.

[9]Wang, J. T.-S., Shaw, D., and Mahrenholtz, O., "Vibration of Rotating Rectangular Plates," *Journal of Sound and Vibration,* Vol. 112, No. 3, 1987, pp. 455–468.

[10]Shaw, D., Shen, K. Y., and Wang, J. T., "Flexural Vibration of Rotating Rectangular Plates of Variable Thickness," *Journal of Sound and Vibration,* Vol. 126, No. 3, 1988, pp. 373–385.

[11]Gupta, K. K., "Development of a Block Lanczos Algorithm for Free Vibration Analysis of Spinning Structures," *International Journal for Numerical Methods in Engineering,* Vol. 26, No. 5, 1988, pp. 1029–1037.

[12]Meirovitch, L., "A New Method for Solution of the Eigenvalue Problem for Gyroscopic Systems," *AIAA Journal,* Vol. 12, No. 10, 1974, pp. 1337–1342.

[13]Bauchau, O. A., "A Solution of the Eigenvalue Problem for Underdamped Gyroscopic Systems with the Lanczos Algorithm," *International Journal for Numerical Methods in Engineering,* Vol. 23, No. 9, 1986, pp. 1705–1713.

[14]Reddy, J. N., and Chao, W. C., "Large-Deflection and Large-Amplitude Free Vibrations of Laminated Composite-Material Plates," *Computers and Structures,* Vol. 13, 1981, pp. 341–347.

[15]Reddy, J. N., and Chao, W. C., "Nonlinear Oscillations of Laminated Anisotropic Rectangular Plates," *Journal of Applied Mechanics,* Vol. 49, 1982, pp. 396–402.

[16]Reddy, J. N., "Geometrically Nonlinear Transient Analysis of Laminated Composite Plates," *AIAA Journal,* Vol. 21, No. 4, 1983, pp. 621–629.

[17]Reddy, J. N., *Energy and Variational Methods in Applied Mechanics,* Wiley, New York, 1984.

[18]Reissner, E., "The Effect of Transverse Shear Deformation on the Bending of Elastic Plates," *Journal of Applied Mechanics,* Vol. 12, No. 12, 1945, pp. 69–77.

[19]Mindlin, R. D., "Influence of Rotatory Inertia and Transverse Shear Deformation on the Flexural Motion of Isotropic, Elastic Plates," *Journal of Applied Mechanics,* Vol. 18, No. 1, 1951, pp. 31–38.

[20]Jones, R. M., *Mechanics of Composite Materials,* Scripta, Washington, DC, 1975.

[21]Bhumbla, R. Reddy, J. N., and Kosmatka, J. B., "A Study of Vibrations in Rotating Laminated Composite Plates Accounting for Shear Deformation and Rotatory Inertia," Virginia Polytechnic Inst. and State Univ., Rept. CCMS-89-15, July 1989.

[22]Reddy, J. N., *An Introduction to the Finite Element Method,* McGraw-Hill, New York, 1984.